International Journal of Mass Spectrometry 371 (2014) 1–7

Contents lists available at ScienceDirect

International Journal of Mass Spectrometry

journal homepage: www.elsevier.com/locate/ijms

A simple electrospray interface based on a DC ion carpet

Staci N. Anthony, Deven L. Shinholt, Martin F. Jarrold *

Chemistry Department, Indiana University, 800 E Kirkwood Avenue, Bloomington, IN 47405, United States

ARTICLE INFO

Article history:
Received 30 October 2013
Received in revised form 9 June 2014
Accepted 9 June 2014
Available online 3 July 2014

Keywords:
Electrospray interface
Ion carpet
Trajectory calculations

ABSTRACT

We describe a simple electrospray interface incorporating a long drift region and a DC ion carpet. The function of the drift region is to thermalize and desolvate the ions. It has a series of ring electrodes supplied with RF and DC voltages, which radially confine and transport ions towards the DC ion carpet. The DC ion carpet consists of a series of concentric rings on a planar printed circuit board, which provide a DC potential gradient that funnels ions through a central aperture. The design and operating parameters were optimized by trajectory calculations and experiments. According to calculations, the transmission efficiency for thermalized ions exceeds 90%, and there is little m/z discrimination at the exit aperture.

1. Introduction

The transport of ions into vacuum has been one of the most prominent areas of sample loss in electrospray mass spectrometry [1]. The transition from atmospheric pressure to low pressure results in a supersonic expansion where heavier species can be accelerated to high energies. Early skimmer interfaces only transmitted ions near the center of the expansion. The development of the ion funnel was an important step forward as it allowed ions to be thermalized, concentrated, and transmitted through a small aperture. The ion funnel consists of a stack of ring electrodes, in which the inner diameter tapers down to a small aperture, supplied with a combination of RF and DC voltages. The first ion funnel afforded an order of magnitude increase in the signal intensity over that obtained with traditional skimmer interfaces [2]. Kim et al. were able to improve the original design to broaden the transmitted m/z range, while Julian et al. were able to relax the physical design constraints regarding the small electrode spacing traditionally used [3,4]. However, the m/z bias inherent in RF-driven devices remains a problem with the ion funnel, especially for low mass (<100 Da) ions, and with the application of high RF amplitudes (>200 V peak-to-peak) [5].

Kanawati et al. have performed an in-depth investigation of the transmission of an ion funnel for a range of m/z values. When optimized, 50% transmission was achieved for ions as low as m/z 80, though no m/z values studied below this point could be transmitted due to the presence of axial traps at the ion funnel exit. Transmission of ions above m/z 1000 was not studied. In addition, the authors noted that the small inner diameters required at the exit of ion funnels (<6 mm) preclude the use of high RF amplitudes because the ions have a higher probability of absorbing energy, becoming defocused, and crashing out [5]. Higher RF amplitudes would be beneficial as they increase the RF pseudopotential that confines the ions radially, thereby increasing transmission.

In 2003, Wada et al. at the RIKEN facility in Japan introduced a different interface design – the RF ion carpet [6]. This interface was developed for nuclear chemistry and physics research where it was used to collect ions from an ion beam after they had been thermalized in a buffer gas. The RF ion carpet (or RF carpet) is a planar printed circuit board with dozens of concentric ring electrodes and a central exit aperture. A linear DC gradient is applied across the electrodes to pull ions into the center of the RF carpet. Two RF signals, 180° out of phase, are applied to adjacent rings to prevent ions from crashing into the circuit board. An ion above the RF carpet obeys the Mathieu equations, in which two dimensionless parameters ($a{-}p^2$ *and* q) describe the stability region [7]. The effect of pressure is incorporated through the unitless parameter p, which accounts for an ion's mobility in the background gas. An analytical solution has also been developed for the dampened pseudopotential generated by an RF ion carpet in a background gas, and this has been used to investigate the stability parameters [8]. It is evident that no matter what operating parameters are chosen, an m/z bias is unavoidable due to the presence of RF potentials.

In addition to the theoretical treatments described above, several experimental investigations have been performed. The effect of space charge on RF carpet performance has been studied, as well as the effects of the pressure and temperature of the background gas [9,10]. An RF ion carpet has been incorporated into an electrospray ionization (ESI) source designed to determine the masses of the

* Corresponding author. Tel.: +1 812 856 1182.
E-mail address: mfj@indiana.edu (M.F. Jarrold).

http://dx.doi.org/10.1016/j.ijms.2014.06.007
1387-3806/

"superheavy" elements [7]. In related work, an "ion surfing" transport method has been proposed and demonstrated. Ion surfing can be performed on either a circular RF carpet or on a strip of printed circuit board with many linear electrodes lying perpendicular to the direction of travel. Multiple phase-shifted RF signals are applied to the electrodes to produce a traveling wave that carries ions along the strip just above the carpet surface [11–13].

Finally, a "planar ion funnel" has been described in a patent application [14]. The planar ion funnel is an ion carpet with concentric rings that are supplied with a DC gradient but no RF voltage. The only characterization reported for this device was a measurement that indicated the transmitted ion current increased as the DC gradient became steeper. The ions were generated by electron impact and the interface was not coupled to a mass spectrometer.

The purpose of this work is to investigate the performance of an ion carpet as an electrospray interface. The interface examined here has a long drift region consisting of circular electrodes supplied with a DC gradient and RF voltages, with an ion carpet placed at the end of the drift region. The long drift region thermalizes and desolvates the ions, which are constrained radially by the RF. At the end of the drift region, the ion carpet transmits the ions through a small aperture. They are subsequently analyzed by a quadrupole mass spectrometer. Simulations indicate that a high ion transmission efficiency can be achieved with only DC voltages applied to the carpet (henceforth called a DC ion carpet or DC carpet), so long as the gradient is large enough and the ions are thermalized. We have investigated how the shape of the electric fields due to the DC voltages on the carpet influences the transmission efficiency. Simulations for a range of different m/z values indicate that there is little m/z bias. Experimental results confirm that, when the gradient is optimized, the DC ion carpet provides a high transmission efficiency.

2. Experimental methods

2.1. Instrument overview

A schematic diagram of the instrument used in these studies is shown in Fig. 1. The ions are generated by electrospray, and then pass through a 0.05 cm inner diameter (ID) heated capillary into the first differentially pumped region. This region contains a 31.6 cm long drift region followed by an ion carpet that separates the first differentially pumped region from the second. The ion carpet can operate in either the DC-only mode or the DC + RF mode. The drift region contains 74 brass ring electrodes with a 2.54 cm ID, spaced 0.381 cm apart. RF signals are applied to the ring electrodes with adjacent electrodes receiving waveforms that are 180° out of phase. The resulting RF fields constrain the ions radially. In addition, a linear DC gradient directs the ions down the drift region towards the ion carpet. The flow of gas through the capillary into this region results in a base pressure of around 0.5 Torr. The pressure can be raised by adding gas to this region through a leak valve. Increasing the pressure increases the residence time in the drift region, which enhances desolvation.

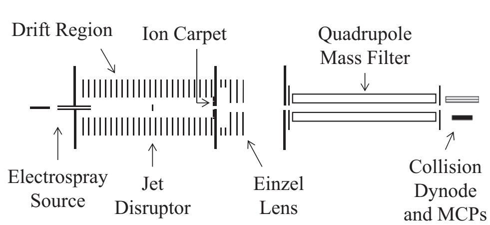

Fig. 1. Schematic diagram of experimental apparatus showing the three differentially pumped regions.

Following the work of Kim et al. [15], a jet disruptor was placed approximately halfway along the drift region. It has been shown previously that an electrode placed directly in the ion's path with a voltage slightly greater than that on the surrounding electrodes will divert ions around the electrode while disrupting the directed gas flow emanating from the capillary inlet. Disrupting this directed gas flow mitigates the gas dynamic effects that could hinder transmission through the exit aperture. The jet disruptor also prevents large droplets, which are accelerated to very high energies in the capillary, from striking and fouling the ion carpet.

The ion carpet is mounted 0.635 cm from the last ring of the drift region with the carpet electrodes facing the drift region. The ion carpet focuses the ions so that they pass through the small aperture at the center of the carpet and enter the second differentially pumped region. The pressure in this second region is approximately 2×10^{-5} Torr. An einzel lens focuses the ions through another aperture and into the third differentially pumped region, where the pressure is approximately 3×10^{-7} Torr. The ions are analyzed by a frequency-scanned quadrupole mass spectrometer and then detected by an off-axis collision dynode and two microchannel plates stacked in a chevron arrangement. A detailed description of the frequency-scanned quadrupole will be provided in a later publication.

The performance of the interface was examined using cytochrome c (horse heart) and bovine serum albumin. The cytochrome c (Sigma–Aldrich) solution was prepared at a concentration of 2 mg/mL in 50:50 water (EMD millipore) and methanol (VWR International) with 2% acetic acid (Mallinckrodt Baker, Inc.) by volume. Bovine serum albumin (Sigma–Aldrich) was prepared at 2 mg/mL in 90:10 water and acetonitrile (J.T. Baker) with 2% acetic acid by volume.

2.2. Ion carpet

The ion carpet is a circular printed circuit board made of Rogers 4003 material. The carpet consists of 24 concentric, gold-plated ring electrodes that are 0.038 cm wide, with 0.013 cm spacing between them. Ions exit through a 0.1 cm diameter hole drilled through the center. The carpet was manufactured by Advanced Circuits (Aurora, Co.). All the electronic components are soldered directly onto the back of the ion carpet, with microvias allowing for electrical connections to the electrodes on the front. An internal ground plane is located between the ring electrodes on the front and electronic components on the back. Two stainless steel plates, one with an o-ring groove, sandwich the ion carpet between them to create a vacuum seal. A photograph of the ion carpet is shown in Fig. 2.

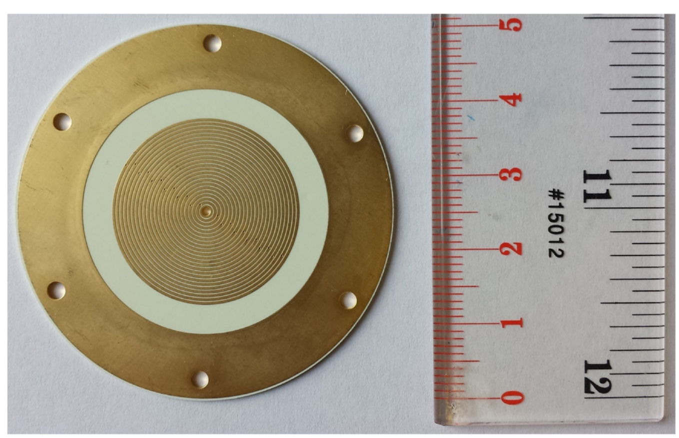

Fig. 2. Photograph of the ion carpet with a ruler to show the scale.

A resistor chain generates a DC voltage gradient across the carpet, with the innermost ring usually held at ground. A more detailed description of the voltage gradient will be given in the next section. In addition, a capacitor chain allows for the addition of RF to the ion carpet. When running in DC carpet mode, the input to the capacitor chain is grounded. There are six evenly spaced holes around the outer edge of the carpet to allow for mounting in the instrument.

2.3. Ion trajectory simulations

SIMION 8.1 was initially used to simulate ion trajectories in the drift region-ion carpet assembly. Two pressure simulation programs are included with SIMION: the hard sphere collision model and the statistical diffusion model. The hard-sphere collision model was too computationally intensive for the desired pressure regime (0.1–1 Torr). In addition, the assumptions regarding movement of an ion due to collisions with a background gas, which are inherent in the statistical diffusion model, precluded the high mass range that we wished to examine [16]. Therefore, SIMION was only used to determine the DC potential and RF electric field at each point in the drift region-ion carpet geometry. The electric field from the RF was then used to calculate the pseudopotential, V^*, at each point, using the following equation,

$$V^* = \frac{zeE_{\mathrm{RF}}^2}{4m\omega^2} \tag{1}$$

where E_{RF} is the net local electric field [17]. This pseudopotential was added to the DC potential to create the total electric field. A Fortran program was then used to simulate ion motion based on the ion's mobility and diffusion. The program assumes a stationary background gas, no initial ion velocity and discounts space charge effects.

Chapman–Enskog theory was used to calculate the diffusion constants. For the case of two rigid, elastic spheres, of diameters σ_1 and σ_2, the first approximation to the diffusion constant, D, is given by [18]:

$$D = \frac{3}{8n\sigma_{12}^2}\sqrt{\frac{k_BT(m_1+m_2)}{2\pi m_1 m_2}} \tag{2}$$

where n is the number density of the background gas, σ_{12} is the average collision diameter, k_B is Boltzmann's constant, T is temperature, and m_1 and m_2 represent the mass of the ion and background gas, respectively. The displacements due to diffusion are modeled in each of the three dimensions by

$$d_{x,y,z} = d_{x,y,z} \pm \sqrt{2\Delta t D} \tag{3}$$

where $d_{x,y,z}$ is the displacement of the ion in the x, y, or z direction and Δt is the time step. The direction of the displacement (+ or −) is chosen randomly. The displacements due to the electric fields in each dimension were calculated using:

$$d_{x,y,z} = d_{x,y,z} + K\Delta t(E_{\mathrm{DC}} + E_{\mathrm{P}})_{x,y,z} \tag{4}$$

in which E_{DC} is the DC component and E_{P} is the pseudopotential component of the electric field in all the three dimensions. The mobility is given by $K = zeD/k_BT$ where ze is the charge on the ion, k_B is the Boltzmann constant, and T is the temperature [19]. The time step was chosen such that the RF was sampled at least 100 times per cycle. A further reduction in the time step did not significantly alter the trajectories.

3. Results

3.1. Ion trajectory simulations

Simulations were first performed to optimize transmission of a wide range of ion masses through the drift region. We did simulations for ions with masses ranging from 100 Da to 1 GDa. The charges were set equal to the Rayleigh limit for a spherical water droplet with the same mass as the ion [20], except for the 100 Da ion where the charge calculated using this approach was 0.57 elementary charges (e). In this case, the charge was rounded up to a realistic value of 1 e. See Table 1 for a list of masses and charges that were used. For each simulation, 500 ion trajectories were calculated at a background gas pressure of 0.5 Torr and a temperature of 298.15 K. The collision cross sections, which are needed to determine the diffusion constants and ion mobilities, were calculated for an 80% N_2/20% O_2 mixture (air) assuming that the ion is spherical and has the same density as water. The radial starting point of the ions was chosen randomly within a 2.0 cm diameter disk centered on the axis of the drift region. The transmission efficiency was determined from the fraction of ions that passed completely through the drift region.

Fig. 3 depicts the percent transmission through the drift region as a function of an ion's m/z for a range of drift region RF frequencies. An RF amplitude of 300 V peak-to-peak (V_{pp}) was applied to the drift region rings, with a drift field of ~0.8 V/cm. It was found that a frequency of 1 MHz was sufficient to ensure ~100% transmission through the drift region for all the ion masses studied. The increased transmission for the 100 Th particle relative to the 600 Th particle for frequencies greater than 1 MHz (see Fig. 3) is due to the rounding up of the charge on the 100 Th ion, which causes a higher pseudopotential. The transmission efficiency is expected to decrease at higher masses because the pseudopotential is inversely proportional to the mass (see Eq. (1)). However, the expected decrease in the transmission efficiency is not observed because the drift region is not long enough for the large ions to diffuse radially to the drift electrodes, where they would be lost.

This explanation can be verified by calculating the average lifetime, τ, of an ion cloud that is expanding due to diffusion to the walls of a container [19]. For the special case of an infinitely long cylinder with a radius r_0, the lifetime is given by

$$\tau = \frac{1}{D}\left(\frac{r_0}{2.405}\right)^2 \tag{5}$$

Table 1
Characteristics of the ions used in the simulations.

Mass (Da)	Charge (z)	m/z	D (cm^2/s)	τ (s)	K (m^2/V s)	v_d (m/s)	l (m)
100	1	100	112	2.49	0.436	33.99	0.085
1000	1.82	550	32.6	8.56	0.231	18.01	0.154
10,000	5.75	1740	8.68	32.1	0.194	15.15	0.487
100,000	18.17	5502	2.09	133.5	0.148	11.52	1.54
1,000,000	57.47	17,400	0.477	584.9	0.107	8.32	4.87
10,000,000	181.74	55,024	0.105	2660	0.074	5.79	15.4
1,000,000,000	1817.39	550,240	0.00498	58,200	0.035	2.75	154

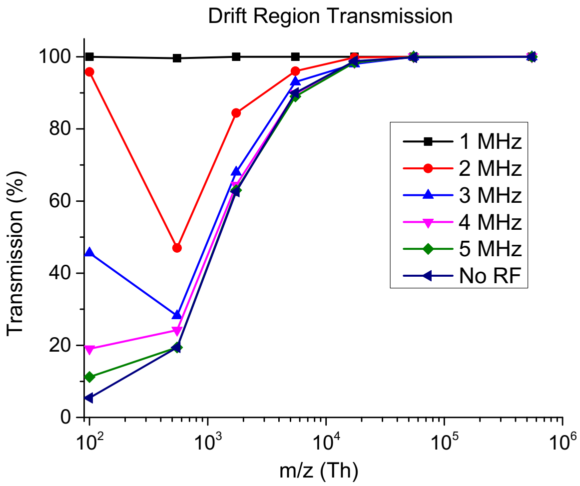

Fig. 3. Drift region transmission of a wide range of ion m/z values as a function of RF frequency. An amplitude of 300 V_{pp} was used for each case. Transmission was determined as the percentage of ions that passed completely through the drift region. At a frequency of 1 MHz, all ions transmitted with an efficiency approaching 100%.

The ion drift velocity, v_d, can be determined from the mobility of the ion and the axial electric field, E, for the drift region.

$$v_d = KE \quad (6)$$

Finally, the average length, l, an ion must travel before colliding with the 'walls' of the drift region can be determined from its average lifetime and drift velocity.

$$l = v_d \tau \quad (7)$$

Table 1 shows the calculated diffusion constants, average lifetimes, mobilities, drift velocities and average drift lengths for each mass and charge combination considered here. The drift length increases as the mass increases. For a mass of 10,000 Da and greater, the average drift length is longer than the drift region. These ions have insufficient time to diffuse to the edge of the drift region. Space charge will enhance the expansion of the ion cloud, so that the actual transmission for high mass ions is likely lower than indicated by the simulations. A decrease in the RF frequency and an increase in RF amplitude would mitigate this ion loss.

We next focused on optimizing the DC gradient applied across the ion carpet. We found that when the carpet DC gradient was relatively large, the transmission efficiency surpassed 90%, with no RF applied to the ion carpet. To maximize the transmission, simulations were performed with three different sets of DC carpet voltages. Examples of the DC potential surfaces extracted from SIMION are shown in Fig. 4. In all cases, a linear gradient of 0.8 V/cm was applied to the drift region. The electric field produced by the DC carpet extends approximately 3 cm into the drift region.

Fig. 4(a) depicts the potential surface resulting from a linear voltage gradient across the DC carpet with the outermost DC carpet ring electrode held at 260 V and the innermost ring at ground. The drift ring closest to the DC carpet is also held at 260 V. Fig. 4(b) shows a non-linear voltage gradient applied to the DC ion carpet, where the field is stronger around the central exit aperture. The voltages on the inner- and outermost DC carpet electrodes are the same as for Fig. 4(a), so the overall voltage drop across the DC carpet is the same. The last drift region ring is held at the same potential as in Fig. 4(a). For Fig. 4(c), the same non-linear gradient is applied to the DC carpet, but the voltage on the last drift ring is reduced to 159 V, 61% of the voltage on the outermost DC carpet electrode. A reduction of this last drift ring voltage, while keeping

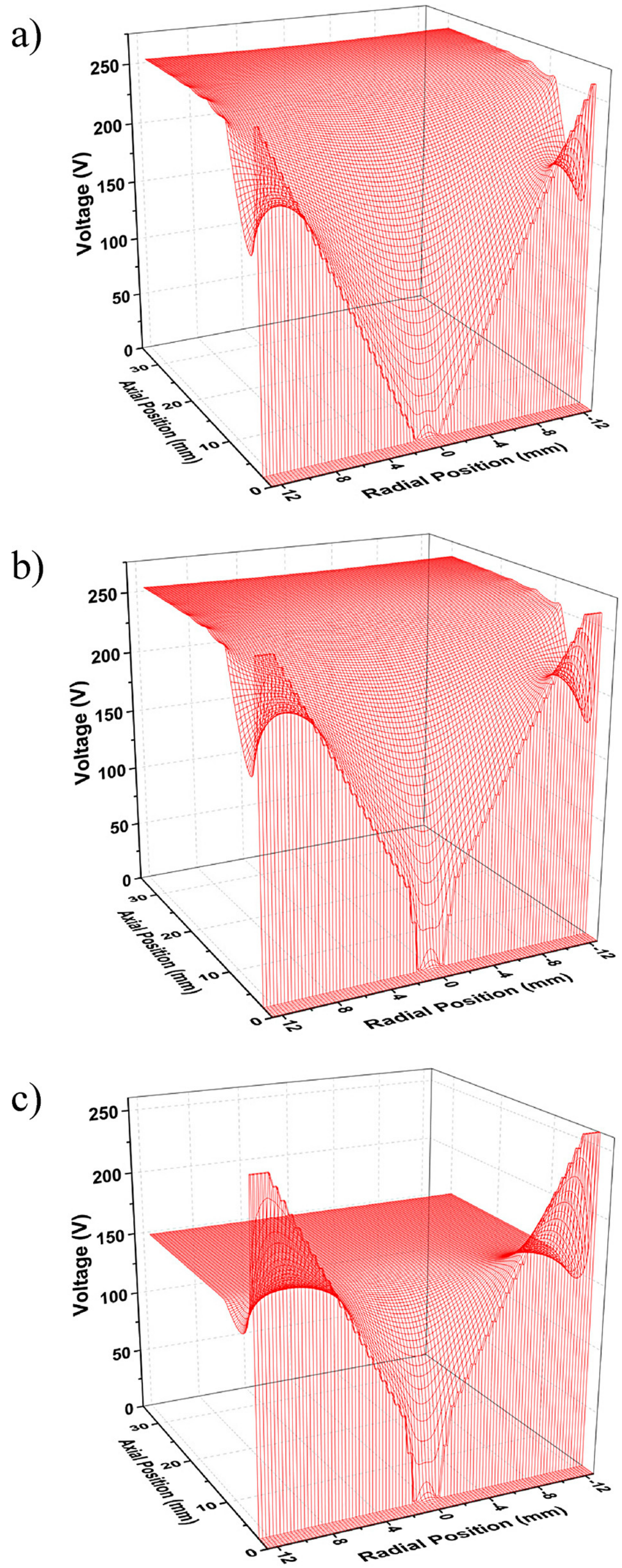

Fig. 4. Contour plots of DC potentials of the ion carpet as a function of axial and radial position. The DC carpet is located at the front of each plot near an axial position of 0 mm. Axial positions beyond this point correspond to the drift region. (a) Shows the potentials that result when a linear gradient is applied to the DC ion carpet. (b) Shows the potentials from a non-linear voltage gradient where the gradient is stronger near the center of the carpet. (c) Shows the potentials from the same non-linear potential as in (b) but with the voltage on the last ring of drift region held at 61% of the voltage on the outermost ring of the DC carpet. In (a) and (b) the voltage on the last ring of the drift region and on the outermost ring of the DC carpet are the same. In all cases, the voltage gradient along the drift region is 0.8 V/cm.

the gradient along the drift region constant, results in the formation of high potential regions at the outer edges of the DC carpet. These high potential regions extend into the drift region, where they strongly repel the ions and push them towards the center. The fields that funnel ions into the central aperture in Fig. 4(c) do not extend into the drift region as far as the fields in Fig. 4(a) and (b), but their onset is sharper.

For each set of voltage gradients we considered, trajectory calculations were performed for 500 ions at a pressure of 0.5 Torr and a temperature of 298.15 K. The RF on the drift region was set to 1 MHz, 300 V_{pp}, values that had been found to transmit almost all ions over a broad range of m/z values. We chose to use a cytochrome c-like particle for these simulations (m = 12,000 Da, z = 13, and a collision cross section of 30.8 nm^2) [21] as cytochrome c was studied experimentally. Transmission was determined as the fraction of ions that pass completely through the innermost ring of the DC carpet. An extraction electrode with a small negative voltage was placed behind the DC carpet to maintain ion motion through the exit aperture. Fig. 5(a–c) shows 20 of the 500 trajectories calculated for the voltage gradients shown in Fig. 4(a–c).

Fig. 5(a) shows trajectories for the linear voltage gradient shown in Fig. 4(a). A transmission efficiency of 84% was obtained with this gradient. Fig. 5(b) shows trajectories obtained with the non-linear voltage gradient shown in Fig. 4(b). It was thought that a non-linear gradient would form a more funnel-shaped potential gradient and improve the ion transmission efficiency, and indeed the transmission efficiency improved to 95%. Finally, the effect of the voltage between the last ring of the drift region and the outermost ring of the DC carpet was examined. In the two examples described above, the last ring of the drift region and the outermost ring of the DC carpet are at the same voltage. For Figs. 4(c) and 5(c) the voltage on the last ring was reduced to 61% of the voltage on the outermost ring. The trajectories are clearly different, with the funneling effect occurring much closer to the DC carpet, and transmission has increased slightly to 98%. As noted earlier, the trajectory calculations do not account for space charge effects, any excess energy possessed by the ions as they enter the drift region, or for the gas flow within the drift region. At the DC carpet end, gas flow probably helps by dragging the ions through the exit aperture, increasing the transmission efficiency. Conversely, space charge will expand the ions radial distribution and reduce the fraction transmitted.

The results described above are for a single mass and m/z value. We next investigated the transmission across a broad range of m/z values (see Table 1 for a list). The non-linear DC gradient from Fig. 4(b) was used for this study. The results are shown in Fig. 6. The fraction transmitted is greater than ~90% for the entire mass range studied. The transmission efficiency decreases slightly as the mass decreases, reaches a minimum at around 600 Th and then increases again. The decrease in the transmission efficiency is mainly due to diffusion in the ion carpet. The increase in the transmission efficiency for the 100 Th ion occurs because the charge for this ion is rounded up.

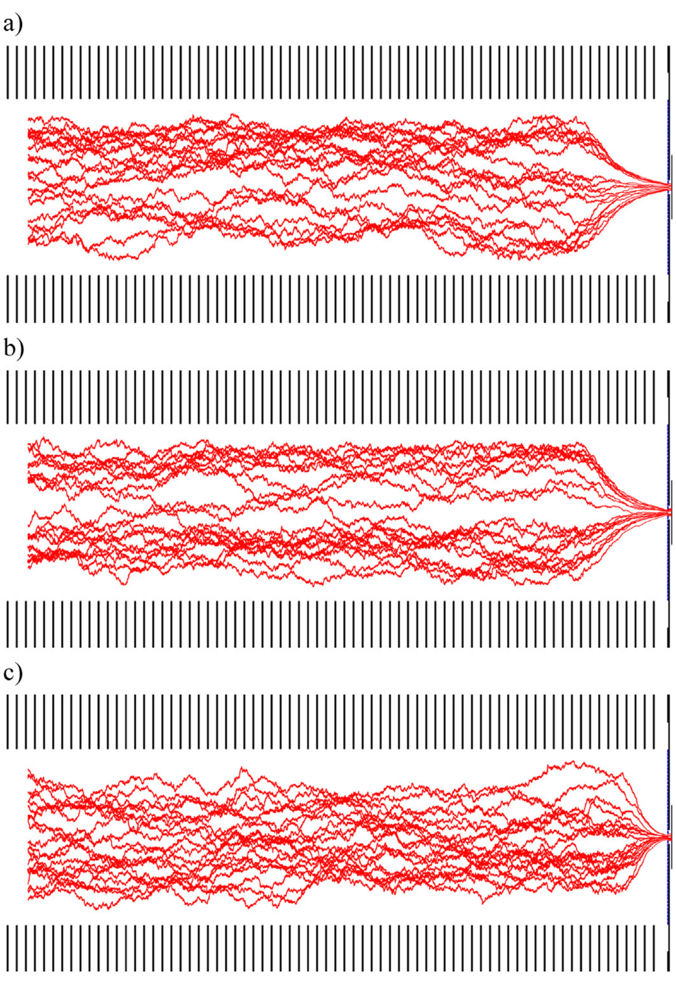

Fig. 5. Trajectory calculations for ions in the drift region–DC carpet interface. Twenty trajectories are shown for each of the three DC carpet voltage gradients shown in Fig. 4. (a) Linear voltage gradient. (b) Non-linear voltage gradient with stronger gradients near the center. (c) Same as (b) but with the voltage on the last ring of the drift region held at 61% of the voltage on the outermost ring of the DC carpet.

4. Experimental results

In the experiments we found that transmission of cytochrome c ions through the drift region was optimized with a slightly higher drift field (~2 V/cm), a slightly higher RF amplitude (400 V_{pp}) and a lower RF frequency (~160 kHz). The higher RF amplitude and lower frequency both lead to a larger pseudopotential suggesting that stronger radial confinement is required in the experiments than in the simulations. This difference may be due to space charge, which is not included in the simulations. Space charge broadens the ions' radial distribution beyond that expected from diffusion alone, and

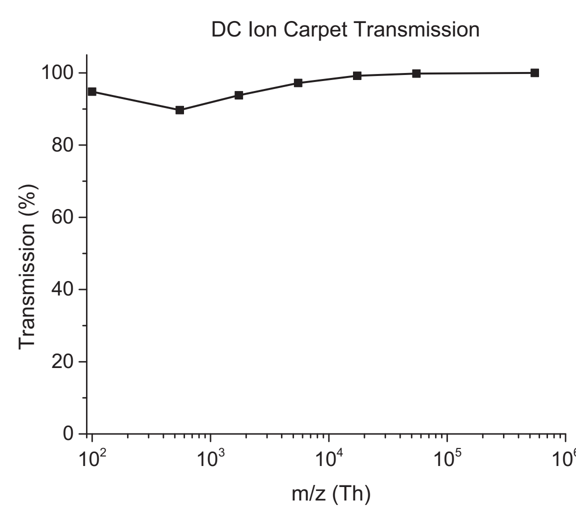

Fig. 6. Transmission efficiency of the DC carpet as a function of m/z. These simulations were performed with the DC carpet gradient from Fig. 4(b). The RF in the drift region was 1 MHz, 300 V_{pp} and the DC gradient was 0.8 V/cm. The transmission efficiency was greater than 90% for all ions studied.

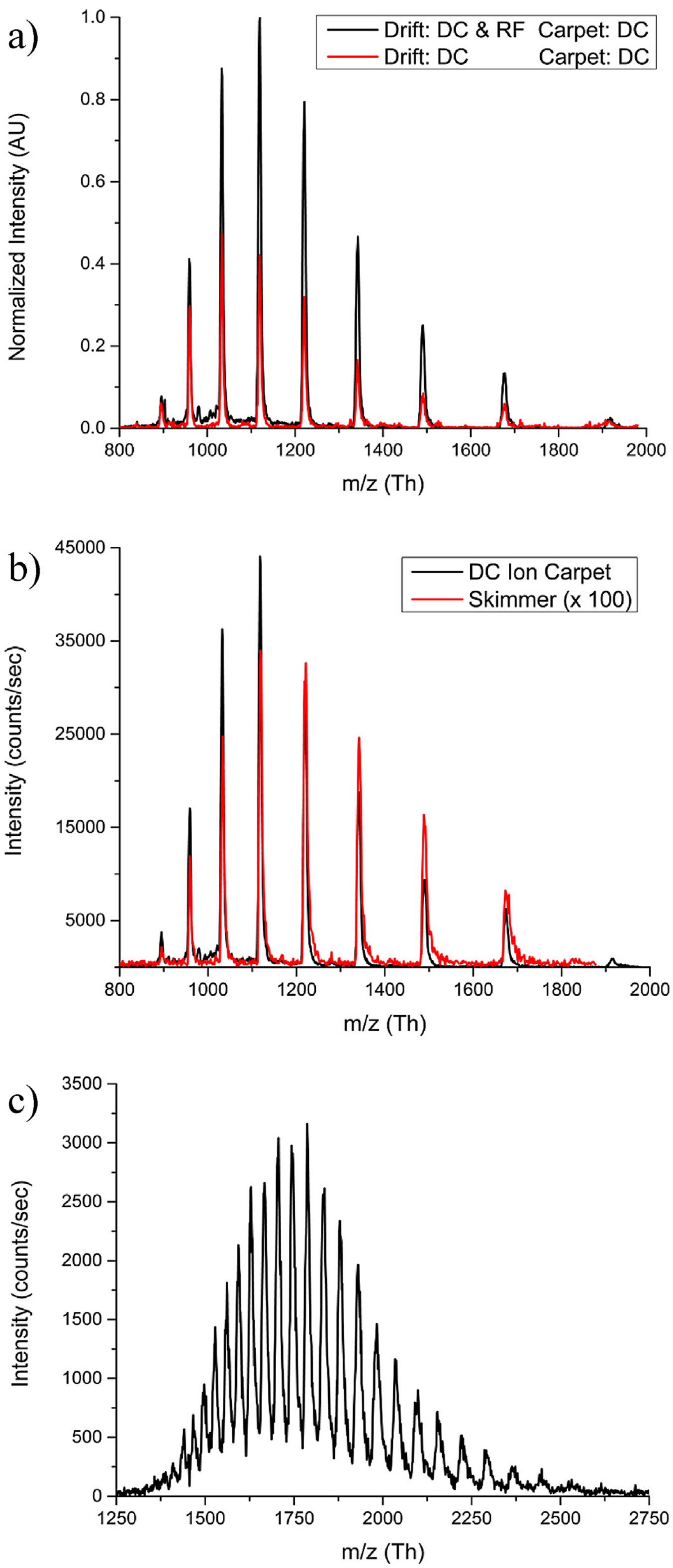

Fig. 7. Cytochrome c mass spectra. (a) The black spectrum was measured with RF and DC applied to the drift region and DC applied to the carpet. The red spectrum shows the effect of removing the RF from the drift region. If the DC is removed from the ion carpet, the transmission efficiency approaches zero. (b) The black spectrum was measured with the DC carpet interface (with RF and DC applied to the drift region) and the red spectrum was measured with the skimmer interface. The intensities of the spectrum measured with the skimmer interface have been magnified 100-fold. The signal from the DC carpet interface is around two orders of magnitude larger than that from the skimmer. (c) Mass spectrum measured for bovine serum albumin, showing the transmission of a large (66.4 kDa) protein.

therefore a stronger confining force is beneficial. In addition, at low RF frequencies, low mass ions can absorb energy from the RF field, and may be lost. Discrimination against very low mass ions, i.e., $(H_2O)_nH^+$, is beneficial in this case because they no longer contribute to the space charge in the ion carpet, allowing more of the ions of interest (in this case, cytochrome c ions at much larger m/z) to be transmitted.

It was also noticed that the ion signal improved significantly when the voltage on the last ring of the drift region was lowered relative to the voltage on the outermost ring of the ion carpet. In other words, the potentials shown in Fig. 4(c) were significantly better in the experiments than the potentials shown in Fig. 4(b), even though the transmission efficiencies from the simulations were similar: 95% for (b) and 98% for (c). This may also be a consequence of space charge. If space charge is important, the delayed funneling evident in Fig. 5(c) is expected to transmit more ions than the more-gradual funneling in Fig. 5(b).

To test the performance of the drift region-ion carpet interface we measured mass spectra for cytochrome c under a variety of conditions. The black trace in Fig. 7(a) is the normalized spectrum measured with the drift region supplied with both DC and RF voltages and the ion carpet supplied with DC voltages. The red trace shows the effect of removing the RF from the drift region: the transmission efficiency drops by more than 50%. If the DC voltages on the ion carpet are removed, essentially no ions were transmitted, which confirms that the DC gradient across the ion carpet is essential for effective transmission of the ions.

The performance of the DC ion carpet was compared to the skimmer interface used previously in this instrument. The same capillary was used for both interfaces, but the drift region is much longer with the carpet interface than with the skimmer. The pressure in the drift region increased from approximately 0.35 Torr with the skimmer to approximately 0.5 Torr with the carpet interface. Fig. 7(b) shows a comparison of mass spectra measured for cytochrome c with both interfaces. The red spectrum was measured with the skimmer interface and has been multiplied by a factor of 100. The black spectrum was measured with the DC ion carpet. Both spectra were collected with the quadrupole operating at the upper tip of the third stability region. The resolving powers for both spectra are similar, with $(m/z)/\Delta(m/z) = \sim 160$. It is evident that the DC ion carpet interface yields around two orders of magnitude more signal.

Even though the simulations indicate that high transmission efficiency is achieved with only DC potentials on the ion carpet. We examined the effect of adding RF to the carpet. The RF carpet amplitude was limited to 150 V_{pp} due to the resistor chain; therefore, a lower RF frequency (900 kHz) was used. We found that adding the RF marginally increased the overall signal (<5%) for cytochrome c. The reason that the RF has such a small effect is that the RF pseudopotential is localized close to the carpet, so the longer-ranged and stronger DC gradient draws the ions to the center of the carpet before they can sense the RF pseudopotential.

Finally, in addition to cytochrome c, we also recorded spectra with bovine serum albumen, a large protein with a mass around 66.4 kDa to test the performance of the interface with much larger ions. A spectrum is shown in Fig. 7(c). Charge states ranging from +26 to +47 are evident. This demonstrates the effective transmission of larger ions by the DC ion carpet. We have also examined smaller ions, we have observed strong signals for Cs^+ and for small $(CsI)_nCs^+$ clusters generated by electrospraying a cesium iodide solution.

5. Conclusions

There are several advantages to the drift region-DC ion carpet combination described here. The spacing between the plates in the drift region is not tightly constrained. This allows for simpler construction of a long drift region, which has a number of advantages, including better thermalization and desolvation of the ions. Simulations indicate that the fraction of ions transmitted by a drift region-DC ion carpet interface exceeds 90% for a wide range of ion masses and that m/z discrimination is small. Finally, experiments show that the drift region-DC carpet interface yields signals that are two orders of magnitude larger than that obtained with a skimmer interface.

Acknowledgement

We gratefully acknowledge the support of the National Science Foundation through grant number 0911462.

References

[1] R.T. Kelly, A.V. Tolmachev, J.S. Page, K. Tang, R.D. Smith, The ion funnel: theory, implementations, and applications, Mass Spectrom. Rev. 29 (2010) 294–312.
[2] S.A. Shaffer, K. Tang, G.A. Anderson, D.C. Prior, H.R. Udseth, R.D. Smith, A novel ion funnel for focusing ions at elevated pressure using electrospray ionization mass spectrometry, Rapid Commun. Mass Spectrom. 11 (1997) 1813–1817.
[3] T. Kim, H.R. Udseth, R.D. Smith, Improved ion transmission from atmospheric pressure to high vacuum using a multi-capillary inlet and electrodynamic ion funnel interface, Anal. Chem. 72 (2000) 5014–5019.
[4] R.R. Julian, S.R. Mabbett, M.F. Jarrold, Ion funnels for the masses: experiments and simulations with a simplified ion funnel, J. Am. Soc. Mass Spectrom. 16 (2005) 1708–1712.
[5] B. Kanawati, K.P. Wanczek, I. Gebefügi, P. Schmitt-Kopplin, Prefocusing inside a linear ion beam guide—a SIMION study, Int. J. Mass Spectrom. 325 (2012) 25–29.
[6] M. Wada, Y. Ishida, T. Nakamura, Y. Yamazaki, T. Kambara, H. Ohyama, Y. Kanai, T.M. Kojima, Y. Nakai, N. Ohshima, A. Yoshida, T. Kubo, Y. Matsuo, Y. Fukuyama, K. Okada, T. Sonoda, S. Ohtani, K. Noda, H. Kawakami, I. Katayama, Slow RI-beams from projectile fragment separators, Nucl. Instrum. Methods Phys. Res. Sect. B 204 (2003) 570–581.
[7] S. Naimi, S. Nakamura, Y. Ito, H. Mita, K. Okada, A. Ozawa, P. Schury, T. Sonoda, A. Takamine, M. Wada, H. Wollnik, An RF-carpet electrospray ion source to provide isobaric mass calibrants for trans-uranium elements, Int. J. Mass Spectrom. 337 (2003) 24–28.
[8] S. Schwarz, RF ion carpets: the electric field, the effective potential, operational parameters and an analysis of stability, Int. J. Mass Spectrom. 299 (2011) 71–77.
[9] A. Takamine, M. Wada, Y. Ishida, T. Nakamura, K. Okada, Y. Yamazaki, T. Kambara, Y. Kanai, T.M. Kojima, Y. Nakai, N. Oshima, A. Yoshida, T. Kubo, S. Ohtani, K. Noda, I. Katayama, P. Hostain, V. Varentsov, H. Wollnik, Space-charge effects in the catcher gas cell of a RF ion guide, Rev. Sci. Instrum. 76 (2005) 1–6.
[10] M. Ranjan, S. Purushothaman, T. Dickel, H. Geissel, W.R. Plass, D. Schaefer, C. Scheidenberger, J. Van de Walle, H. Weick, P. Dendooven, New stopping cell capabilities: RF carpet performance at high gas density and cryogenic operation, Europhys. Lett. 96 (2011) 52001.
[11] G. Bollen, "Ion surfing" with radiofrequency carpets, Int. J. Mass Spectrom. 299 (2011) 131–138.
[12] M. Brodeur, A.E. Gehring, G. Bollen, S. Schwarz, D.J. Morrissey, Experimental investigation of the ion surfing transport method, Int. J. Mass Spectrom. 336 (2013) 53–60.
[13] F. Arai, Y. Ito, M. Wada, P. Schury, T. Sonoda, H. Mita, Investigation of the ion surfing transport method with a circular rf carpet, Int. J. Mass Spectrom. 362 (2014) 56–58.
[14] F.H.W. van Ameron, A. Chaudhary, R. T. Short (SRI International, USA). Planar Ion Funnel. US Patent 20,130,120,894, May 16, 2013.
[15] T. Kim, K. Tang, H.R. Udseth, R.D. Smith, A multicapillary inlet jet disruption electrodynamic ion funnel interface for improved sensitivity using atmospheric pressure ion sources, Anal. Chem. 73 (2001) 4162–4170.
[16] A.D. Appelhans, D.A. Dahl, SIMION ion optics simulations at atmospheric pressure, Int. J. Mass Spectrom. 244 (2005) 1–14.
[17] H.G. Dehmelt, Radiofrequency spectroscopy of stored ions I: storage, Adv. At. Mol. Phys. 3 (1967) 53–72.
[18] S. Chapman, T.G. Cowling, The Mathematical Theory of Non-uniform Gases: an Account of the Kinetic Theory of Viscosity, Thermal Conduction and Diffusion in Gases, Cambridge University Press, New York, 1970.
[19] E.A. Mason, E.W. McDaniel, Transport Properties of Ions in Gases, Wiley, New York, 1988.
[20] Lord Rayleigh, On the equilibrium of liquid conducting masses charged with electricity, Philos. Mag. 14 (1882) 184–186.
[21] M.F. Bush, Z. Hall, K. Giles, J. Hoyes, C.V. Robinson, B.T. Ruotolo, Collision cross sections of proteins and their complexes: a calibration framework and database for gas-phase structural biology, Anal. Chem. 82 (2010) 9557–9565.